Observational Study

Medicine®

OPEN

Evaluation of the anatomic and hemodynamic abnormalities in tricuspid atresia before and after surgery using computational fluid dynamics

Li-Jun Chen, MD[a], Yu-Qi Zhang, MD[a,*], Zhi-Rong Tong, MS[b,c], Ai-Min Sun, MD[d]

Abstract

Analysis of hemodynamics inside tricuspid atresia (TA) chamber is essential to the understanding of TA for optimal treatment. In this study, we introduced a combined computational fluid dynamics (CFD) to simulate blood flow in the left ventricle (LV) to study the diastolic flow changes in TA.

Real-time 3-dimentional echocardiography loops (ECHO) were acquired in normal control group, in TA patients before surgery (pre-op group) and after surgery (post-op group). ECHO loops were reconstructed and simulated by CFD, the geometric, volumetric changes, and vortices in the LV were studies and compare among 3 groups.

Compared with the control group, pre-op TA patients demonstrated significant LV remodeling, manifesting with smaller LV length, larger diameter, width and spherical index, as well as lager volumes; post-op TA group showed revisions in values of both geometric and volumetric measurements. CDF also demonstrated the abnormality of vortices in the pre-op TA patients and the alteration of existence and measurements of vortex in postoperation group.

Echo-based CFD modeling can show the abnormality of TA in both LV geometric, volumetric measurements and intracardiac vortices; and CFD is capable to demonstrate the alterations of LV after Fontan and Glenn surgical procedure.

Abbreviations: 3D = 3-dimensional, CFD = computational fluid dynamics, D_{LV} = diameter of the LV, ECHO = echocardiography, EDV = end diastolic volume, EF = ejection fraction, EPIV = echo particle imaging velocimetry, ESV = end systolic volume, I_D = index of the diameter, I_L = index of length, I_{LD} = index of longitudinal distance, IRB = institutional review board, I_{RD} = index of radial distance, LD = longitudinal distance, L_{LV} = length of LV, LV = left ventricle; left ventricular, MR = magnetic resonance, Post-op = patients after surgery, Pre-op = patients before surgery, RD = radial distance, REC = research ethics committee, RV = right ventricle; SI = spherical index, TA = tricuspid atresia, VFM = vector flow mapping, V_{LV} = volume of the LV, W_{LV} = width of the LV.

Keywords: computational fluid dynamics, Fontan, Glenn, intraventricular hemodynamics, tricuspid atresia

1. Introduction

Tricuspid atresia (TA) is a congenital heart disease, in which the tricuspid valve fails to develop, causing a block from the right atrium to the right ventricle (RV). The absence of right atrioventricular connection in TA leads to a hypoplastic RV, a right-to-left shunting, and an overbearing left ventricle (LV), which receives and pumps the admixture of all systemic venous and pulmonary venous return. Hemodynamic loads are indispensable in the process of the cardiac remolding, which generally accepted as a determinant of the clinical course of heart failure.[1] Surgeries such as Glenn and Fontan can improve the long-term outcomes of TA,[2] but ventricular failure related late deaths still affect its mortality.[3] Therefore, it is critical to evaluate the anatomical and functional abnormalities of the LV, and to study the intracardiac hemodynamics before and after surgery.

In recent years, echo particle imaging velocimetry (EPIV), vector flow mapping (VFM), and magnetic resonance (MR) velocity mapping have been applied to analyze the intraventricular hemodynamics. However, the low spatial resolution and only 2-dimensional flow field analysis of EPIV[4]; the angle dependence and low frame rate of VFM,[5] and the time-consuming scanning and poor temporal resolution of MR,[6] limit the accuracy of them and their applications.

Over the last couple of decades, medical image-based computational fluid dynamics (CFD) has been widely employed to provide intraventricular flow information. CFD is a methodology combining numerical methods with computer simulation that can quantify the flow field. With the development of 3D reconstruction software, CFD has been applied to study the characteristics of flow in the blood vessel [7,8] and ventricle [9,10]; it has been proved to be capable of providing valuable detailed information that can assist on the assessment of heart performance and diagnose of heart dysfunction at an early stage.[10] Although CFD simulations indicate that the effect of intraventricular blood flow pattern on the pumping power is physiologically insignificant,[11] the CFD simulations of the abnormal flow patterns on ventricular function and mechanical efficiency in TA remain open to inquiry. Therefore, the aim of this

Editor: Manal Elshmaa.

All of the authors take full responsibility for all aspects of the reliability and freedom from bias of the data presented, and their discussed interpretation. The authors report no conflicts of interest.

[a] Department of Pediatric Cardiology, [b] Department of Cardiothoracic Surgery, [c] Institute of Pediatric Translational Medicine, [d] Department of Medical Imaging, Shanghai Children's Medical Center, Shanghai Jiaotong University School of Medicine, Shanghai, China.

[*] Correspondence: Yu-Qi Zhang, Shanghai Children's Medical Center, 1678 Dongfang Road, Shanghai 200127, China
(e-mails: jinlong_liu_man@163.com, zyq6812@sina.com).

Medicine (2018) 97:2(e9510)

Received: 9 August 2017 / Received in final form: 14 November 2017 / Accepted: 8 December 2017

http://dx.doi.org/10.1097/MD.0000000000009510

Table 1

Clinical characteristics of study subjects in 3 groups.

	Control	Pre-op	Post-op
Age, mo	30±16	30±17	37±17
Gender (M/F)	7/6	7/6	7/6
Weight, kg	13.87±3.56	12.42±4.48	13.76±4.44
Height, cm	93.71±14.68	89.42±18.70	92.85±17.68
SpO_2 (%)	99±0.2[*,†]	76±7 [*,‡]	83±6 [†,‡]
Systolic BP, mm Hg	79±6 [†]	83±8 [‡]	86±6 [†,‡]
Diastolic BP, mm Hg	53±5	51±6 [‡]	56±5 [‡]

BP = blood pressure, M/F = male to female ratio, SpO_2 = blood oxygen saturation level.
$P < .05$ is statistically significant.
[*] Pre-op versus normal.
[†] Post-op versus normal.
[‡] Post-op versus pre-op.

study is to reveal the capability of CFD in simulating the anatomic and hemodynamic abnormalities in TA.

2. Methods

2.1. Study subjects

Fourteen patients diagnosed with TA using echocardiography, computed tomography, and confirmed by surgery were recruited at the Shanghai Children's Medical Center of Shanghai Jiaotong University School of Medicine from August 2013 to May 2017. Patients with serious arrhythmia, heart failure, and systemic and metabolic conditions, which could adversely affect the cardiac structure and function, were excluded. All the patients did not take any drugs that would affect cardiac contractility. All the surgical procedures were performed by the same surgical team. Echocardiography examinations were performed before Glenn or Fontan operation (pre-op group) and after operation within 6 to 10 months (post-op group). One patient was excluded because of bad echocardiography image quality. Thirteen age- and gender-matched normal children were recruited in the study as the normal control group (Table 1). The parents of all the study subjects have signed informed consent, and the study was approved by the local institutional review board (IRB) and regional research ethics committee (REC) of Shanghai Children's Medical Center Affiliated to Shanghai Jiaotong University School of Medicine, in accordance with the requirements of the implementation of the Helsinki declaration. All the study design, manner of data collection, and data analysis in this study were performed in accordance with the guidelines and regulations of IRB and REC.

2.2. Image acquisition and analysis

A Philips iE33 ultrasonic diagnostic apparatus (Philips, Andover, MA), equipped with an X7–2 or X5–1 probe, was used to acquire full-volume image loops. The standard echocardiographic assessment was performed according to the American Society of Echocardiography Guidelines.[12,13] During acquisition, all subjects were in the left lateral decubitus position, with electrocardiogram recorded simultaneously. The image loops were stored in a hard drive for further CFD reconstruction and analysis.

Tomtec 4D Cardio-View 3 (Tomtec Imaging Systems GMBH, Unterschleisheim, Germany) was applied for post-processing analysis. Primary analyses were performed by manual border tracking in 3 planes (2-chamber, 3-chamber, and 4-chamber), and then end-diastolic volume (EDV), end-systolic volume (ESV), and ejection fraction (EF) were automatically calculated by the software. Images that were not satisfied with tracking could be manually modified and analyzed again.

2.3. CFD Reconstruction, meshing, and simulation

The process of CFD reconstruction, meshing, and simulation is shown in Fig. 1. Full-volume echo image loops with a temporal

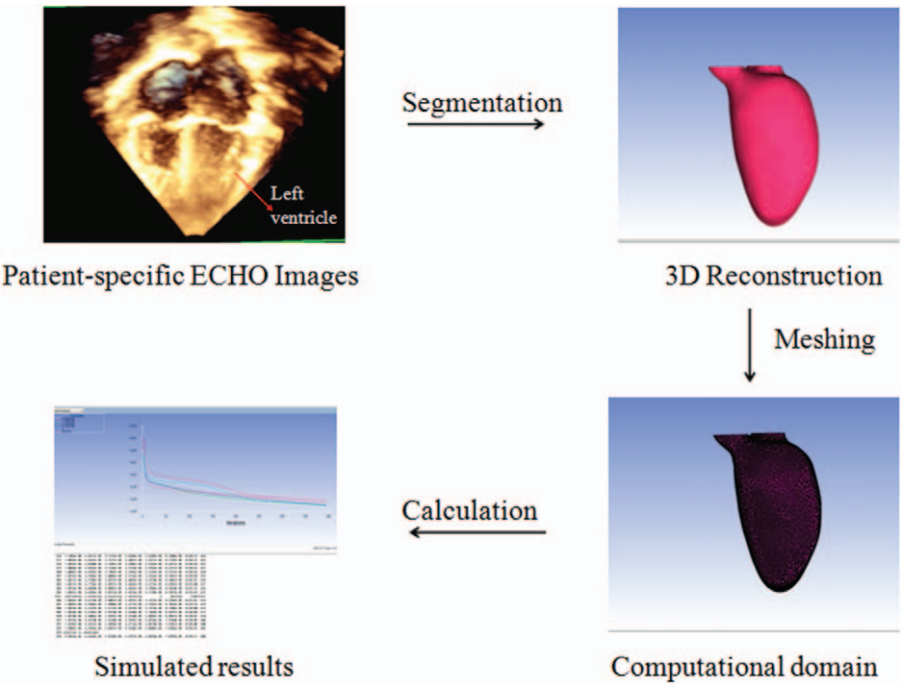

Figure 1. The process of 3D model reconstruction, meshing and CFD simulation. Patient-specific real-time 3D echocardiography image loops were used for CFD reconstruction of LV, meshing, and then simulated.

resolution greater than 27 frames per second were imported into Materialise-Mimics 19.0 (Plymouth, MI) for processing. The layer thickness of the echo images was 0.49 mm, which provided detailed information for CFD reconstruction than any other image modalities. At first, the "Thresholding" tool determines gray scale value ranging to include all the cardiac tissue information, including left ventricular and atrial walls, mitral and aortic valve, and ascending aorta. Both the "Multiple slice edit" and "Edit masks" tool can be used for manual adjustment optimize tissue tracing. The "Region growing" tool was applied to generate mask; the "Calculate 3D from mask" tool was applied to generate 3D model. At last, the "Smooth mask" tool was used for surface smoothing to optimize the CFD 3D heart model.

The cardiac anatomy was determined by echocardiography and then represented by 5 body-fitted prism layers as boundaries ANSYS-ICEM 17.0 (ANSYS, Inc.) for numerical solutions of the Navier–Stokes flow equations. The distance from the first layers to the model surface was 0.02 mm, with 1,000,000 to 3,000,000 tetrahedral mesh elements filling the remaining of the calculated domain. The computational domain was extended to include the proximal atrium and ascending aorta or pulmonary artery for accurate simulation and calculation. The simulation was accomplished by using the ventricular geometry for reconstruction and the velocities of inflow/outflow as boundary conditions. As described in other simulations of ventricular flow studies,[14–17] in this CFD model, the dynamic valvular motion was not calculated independently with the ventricular walls; similarly, the LV endocardium was smoothed in the simulated model.

At isovolumic relaxation, the ventricular muscle continues to relax for about 0.03 to 0.06 second, and the intraventricular pressures drops rapidly from about 80 mm Hg to almost 0 mm Hg; then follows the early diastole (ED), with a flow velocity around 1.2 m/s. The blood in the LV is assumed to be an incompressible Newtonian fluid with a constant viscosity of 0.004 kg/ms and density of 1060 kg/m^3. According to the formula of Reynolds index: $Re = \rho UD/\mu$, its Reynolds number >4000, so it is considered to turbulence. Therefore, the standard k–ε model was applied to solve the motion of intraventricular blood flow; this model is a 2-equation eddy viscosity model based on the solution of equations for the kinetic energy of turbulence and turbulence dissipation rate. The second-order up-wind scheme was employed to complete the steady-state numerical simulation by ANSYS-FLUENT 17.0 software. Finally, boundary conditions from the ECHO data were applied to the finite volume solver package to complete the simulation. When analyzing the vortex during the filling phase, the walls of the models were assumed to be rigid.

After the CFD simulation was completed, the following parameters were calculated: index of the length of main vortex (I_L, the ratio between the length of the main vortex and the length of the LV), index of the diameter of main vortex (I_D, the ratio between the diameter of the main vortex and the diameter of the LV), longitudinal distance index of main vortex ($I_{LD} = LD/L_{LV}$, LD: the longitudinal distance from the center of the main vortex to the mitral annulus, L_{LV}: the longitudinal distance from apex to the base of LV), and radial distance index of main vortex ($I_{RD} = RD/D_{LV}$, RD: the radial distance from the center of the main vortex to the left ventricular long axis, D_{LV}: the distance from septum to the posterior wall at mid-ventricular level).

2.4. Validation

After the reconstruction was completed, quantified measurements were obtained from the CFD reconstructed results, and then compared with echocardiography measurements. In the apical 4-chamber view, the distance from LV apex to base was acquired as the maximum length (L_{LV}), the distance from septum to the lateral wall at the LV mid-ventricular level was acquired as the diameter (D_{LV}), and the volume (V_{LV}) of the LV were acquired by tracing the endocardial borders. The distance from the septum to the posterior wall was acquired as the LV width (W_{LV}) at the mid-ventricular level in the parasternal view. In addition, the spherical index (SI) of the LV was calculated from the ratio between the diameter and length. In the meantime, EDV, ESV, stroke volume (SV), and EF were calculated. Bland–Altman analysis was performed to compare inter-technique agreements between CFD reconstructed measurements and ECHO measurements to validate the CFD method.

2.5. Statistical analysis

Statistical Package for Social Sciences (SPSS 17.0; SPSS Inc, Chicago, IL) was applied for statistical analysis. Numerical variables were presented as mean ± standard deviation. *T* test was performed to test the differences between groups. Bland–Altman analysis was used to test the agreement between CFD measurements and Echo-derived values. All statistical tests were 2-sided, and $P < .05$ was set for statistical significance.

3. Results

3.1. Clinical characteristics

The age, gender, weight, and height of normal control group and the pre-op group were comparable (*all* $P > .05$) (Table 1). Among the 13 patients with TA, 9 of them went through the Fontan procedure and 4 went through the Glenn procedure. Three of the 4 patients who had the Glenn procedure went through the Fontan procedure 16 to 24 months later. The thoracic drainage tube was placed in all of the patients for 7.38 ± 2.69 days. The pulmonary artery pressure was acquired via intracardiac catheterization in 11 pre-op TA patients and 4 post-Glenn procedure patients. The average pulmonary artery pressure of the 11 TA patients was 14.36 ± 2.77 mm Hg and the average pulmonary artery pressure of the 4 post Glenn procedure patients was 17.75 ± 3.86 mm Hg. The blood oxygen saturation level (SpO_2) was significantly low in the pre-op patient group (76.69 ± 7.05%) when compared with the normal control group (99.92 ± 0.28%). The SpO_2 level improved in the post-op group (83.23 ± 5.67%) when compared with pre-op group (76.69 ± 7.05%), but still under normal level (99.92 ± 0.28%) by the time of the follow-up study. The systolic pressure values were higher in the TA pre- and post-op patients' group than in the normal control group, even though only the post-op group demonstrated significant differences ($P = .004$). However, the diastolic pressure values were lower in the pre-op group than both normal control group and the post-op group, with only the significance was only found in between the pre-op and the post-op group ($P = .034$).

3.2. Anatomic assessments of TA patients before and after surgery versus normal control

The geometric and volumetric measurements can be derived from the CFD-reconstructed ECHO images. Compared with the normal control group, the pre-op and post-op group demonstrated larger values in geometry measurements during early and late diastole. During ED, the pre-op and post-op group both

Table 2

CFD-derived left ventricular geometric and volumetric measurements in 3 groups during diastole.

	Control	Pre-op	Post-op
V_{ED}, mL	21.39 ± 5.34	27.09 ± 8.74	25.10 ± 9.12
L_{LVED}, cm	4.22 ± 0.56	3.91 ± 0.48	3.92 ± 0.46
D_{LVED}, cm	2.78 ± 0.35*,†	3.25 ± 0.32*	3.10 ± 0.28†
W_{LVED}, cm	3.12 ± 0.38	3.30 ± 0.36	3.08 ± 0.40
SI_{ED}	0.66 ± 0.03*,†	0.84 ± 0.08*	0.80 ± 0.06†
L_{LVLD}, cm	4.59 ± 0.59*,†	4.06 ± 0.51*	4.14 ± 0.47†
D_{LVLD}, cm	3.11 ± 0.31*,†	3.64 ± 0.32*	3.54 ± 0.29†
W_{LVLD}, cm	3.21 ± 0.28*,†	3.70 ± 0.43*	3.56 ± 0.46†
SI_{LD}	0.68 ± 0.03*,†	0.90 ± 0.08*	0.86 ± 0.08†
EDV, mL	32.27 ± 7.60*	40.64 ± 10.09*	37.06 ± 11.05
ESV, mL	12.56 ± 2.94*	16.11 ± 3.79*	14.63 ± 3.95
SV, mL	19.71 ± 4.75*	24.52 ± 6.52*	22.42 ± 7.21
EF (%)	61.10 ± 1.59	60.15 ± 2.59	60.10 ± 2.44

D_{LVED} = diameter of the left ventricle during early diastole, D_{LVLD} = diameter of the left ventricle during late diastole, EDV = end-diastolic volume, EF = ejection fraction, ESV = end-systolic volume, L_{LVED} = length of the left ventricle during early diastole, L_{LVLD} = length of the left ventricle during late diastole, post-op = patients with tricuspid atresia after operation, pre-op = patients with tricuspid atresia before operation, SI_{ED} = spherical index during early diastole, SI_{LD} = spherical index during late diastole, SV = stroke volume, V_{ED} = volume during early diastole, W_{LVED} = width of the left ventricle during early diastole, W_{LVLD} = width of the left ventricle during late diastole.

$P < .05$ is statistically significant.

* Pre-op versus control.

† Post-op versus control.

demonstrated larger LV diameters (D_{LVED}, $P < .05$) and SI ($P < .001$) (Table 2); the diameters and the SI both showed decreases in values after surgical procedures. During late diastole, when compared with the normal control group, the TA group showed smaller values in length, and bigger values in diameter and width (all $P < .05$), along with a significantly increased SIs value of LV ($P < .001$). Post-op group showed insignificant improvement in SI values, along with longer length, smaller diameter, and smaller width in LV when compared with pre-op group. Compared with the normal control group, the pre- and post-op groups both demonstrated increase in volume measurement, as manifested as significant larger EDV, ESV, and SV in the pre-op group (all $P < .05$), and a decrease in values post-op. Furthermore, Bland–Altman analyses demonstrated good concordance between the CFD measured values and Echo-derived measurements, in terms of diameters and volumes. The interclass correlations (ICCs) for volume and diameter measurements were 0.93 and 0.94, respectively (Fig. 2).

3.3. Intra-cardiac hemodynamic assessment of TA patients before and after surgery versus normal control

CFD enables the visualization of intracardiac flow; flow property can be semi-quantified with color-coded velocity. In this study, CFD was used to demonstrate the blood flow streamlines of normal LV and the LV of the TA patients' pre-op and post-op (Fig. 3). During the filling period, LV pressure drops, when the pressure in the LV is lower than the left atrial (LA) pressure, the mitral valve opens, blood flows into the LV from the LA, and forms a main vortex with counter-clockwise rotation. In the normal LV, the vortex was located below the mitral annulus and close to the lateral wall, occupying the substantial chamber of the LV. A small vortex was observed at corner between the inflow tract and the outflow tract with clockwise rotation. The small corner vortex appeared later than the main vortex, and both the vortices persistent throughout diastole.

The main vortex was observed in only 11 patients (85%) in the pre-op group but appeared in all of the 13 patients (100%) after surgery. Furthermore, the vortex in the pre-op group was closer to the LV base region in position when compared with the normal control group. In regard to the small vortex presented at corner between the inflow tract and the outflow tract in the normal LV, it was only observed in 1 patient (8%) during late diastole and 2 patients (15%) during ED in the pre-op group and 3 patients (23%) during late diastole in the post-op group.

In the ED, the TA patients demonstrated smaller diameter (I_D) of the main vortex when compared with the normal control group ($P = .015$). In the late diastole, the length (I_L), and the diameter (I_D) of the main vortex in the TA pre-op and post-op groups were significantly smaller than in the normal control group (all $P < .05$). The pre-op TA patients group showed significant smaller circularity index (CI) of the main vortex when compared with the normal control group ($P = .027$); however, the post-op group showed a significant increase in CI values when compared with the pre-op group ($P = .028$) (Table 3).

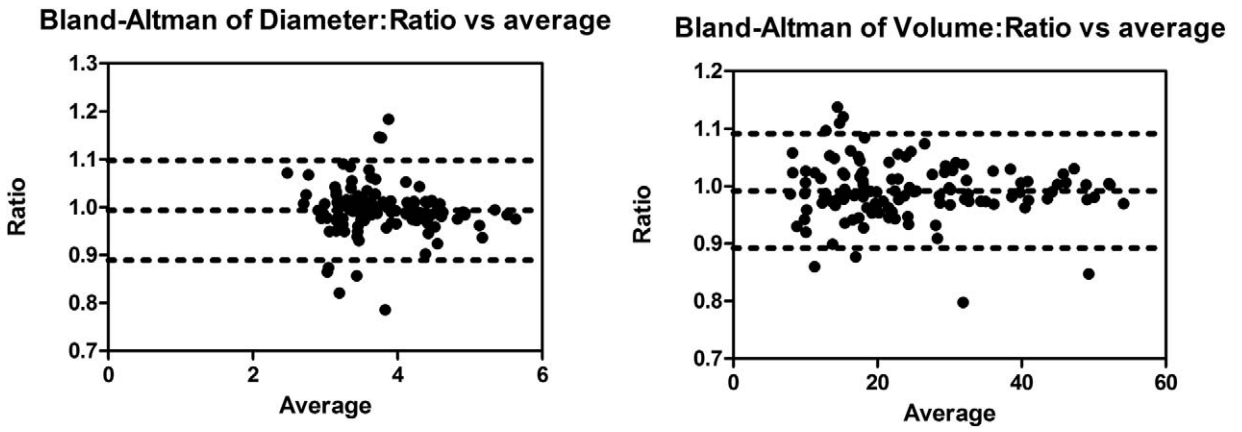

Figure 2. Bland–Altman analysis of diameter and volume between CFD and echocardiography measurements. (left: Bland–Altman analysis of diameter measurements; right: Bland–Altman analysis of volume measurements).

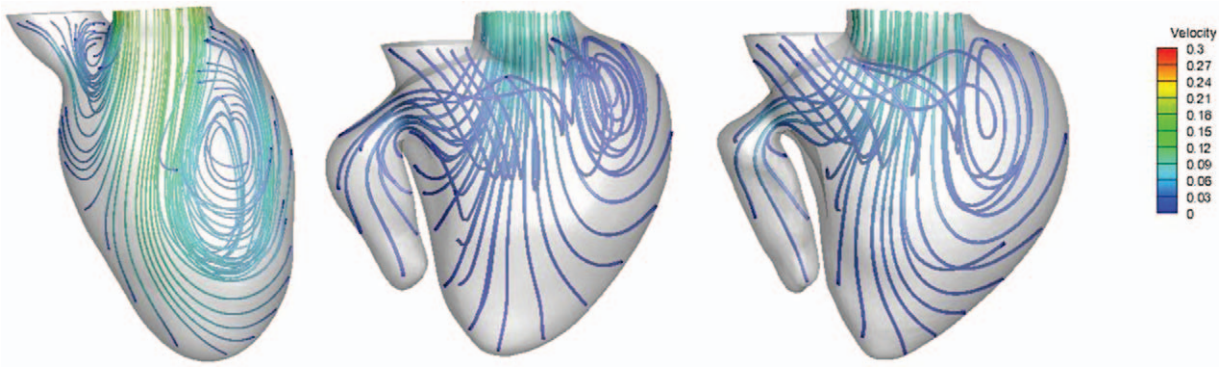

Figure 3. Streamline in the normal LV and TA patients before and after operation during diastole. (A: streamlines in normal left ventricle during early diastole; B: streamlines in TA before operation during early diastole; C: streamlines in TA after operation during early diastole; D: streamlines in normal left ventricle during late diastole; E: streamlines in TA before operation during late diastole; F: streamlines in TA after operation during late diastole).

4. Discussion

TA has abnormal systolic and diastolic function.[18] Evaluating its function before and after surgery is conducive to the preoperative diagnosis, surgical strategy, postoperative follow-up, and prognosis. Therefore, accurate and simple quantitative evaluation of the blood flow is essential to the comprehension of ventricular function.

Clinically, the TA patients showed significant decrease in blood oxygen saturation level but improved after surgery, which is a significant manifest of the efficiency of surgery. Even though the systolic and diastolic blood pressure values were higher in the post-op group, but all the blood pressure values were in the normal range of the patients' ages. The increase of blood pressure after surgery might be a sign of increased systemic vascular resistance.[2,19–21]

TA is characterized primarily by complicated anatomy, chronic hypoxia, and increased blood viscosity, together with changes in heart capacity and load, causing LV chamber to expand. Volumes increase as a response of adaptive to maintain the SV and normal cardiac output. After this early compensative stage, the process is driven predominantly by enlarged ventricular chamber and a shift from an elliptical to a more spherical chamber configuration.

During early systolic dysfunction, the ventricle enlarges with greater increase of the short axis than the long axis (sphericity), the spherical change may help the ventricle to compensate by increasing the volume to maintain normal SV. Gradually, the LV remodeling promotes the deterioration of ventricular function, and eventually advancing heart failure.[22] This remodeling and deterioration of the LV can be stopped or reversed after palliative surgery such as Fontan operation. The LV remodeling of TA was manifested as the changes in LV length, diameter, width, and SI. The length of the LV in the TA pre-op group was smaller than in the normal control group, and showed an increase in value in the post-op group ($P < .05$). The diameter and the width of the LV were larger in the TA pre-op group than the normal control, and demonstrated a decrease in the post-op group ($P < .05$). Both diameter and width increase in TA patients was the manifestation of the increase of sphericity of LV, so was the SI values ($P < .05$). All of the CFD-derived geometric evidence of LV remodeling in TA patients were improved after surgery.

Right ventricular chamber in TA had small capacity, along with the existence of septal defect, resulting in the compensatory expansion and volume overload of left ventricular chamber; therefore, the volumes of patient (EDV, ESV, SV) were larger than that of normal. After Glenn or Fontan operation, the blood of vena cava was directly shunt to the pulmonary artery, capacity load of LV was alleviated; therefore, the LV volume decreased, but still larger than that of normal LV volume. CFD-derived volumetric measurements were sufficient to reveal the pathological changes of TA and the turnaround of LV after surgery. In addition, the qualitative comparisons on L_{LV}, D_{LV}, W_{LV}, EDV, ESV, and SV showed good correspondence between the CFD-reconstructed results and ECHO measured values, which identified the reliability of CFD methodology in measurement of diameters and assessment on cardiac functions.

The left ventricular diastolic filling process is an active process, which plays a very important role in the function of the heart.[22] As diastolic flow inside the ventricular chamber is dominated by strong vortices, spatiotemporal tracking and analysis of vortices with CFD provide both quantitative and qualitative flow data that can be related to ventricular physiology.[22] Diastolic vortices store momentum and release it during ejection. Dissipation of

Table 3

Characteristics of vortices among 3 groups during diastole.

	Control	Pre-op	Post-op
I_{LED}	0.60 ± 0.09	0.47 ± 0.18	0.57 ± 0.16
I_{DED}	0.46 ± 0.12*	0.30 ± 0.17*	0.38 ± 0.15
I_{LDED}	0.39 ± 0.02	0.38 ± 0.07	0.38 ± 0.07
I_{RDED}	0.28 ± 0.02	0.26 ± 0.08	0.28 ± 0.05
CI_{ED}	0.53 ± 0.11	0.52 ± 0.15	0.54 ± 0.14
I_{LLD}	0.70 ± 0.03*,†	0.48 ± 0.18*	0.54 ± 0.21†
I_{DLD}	0.51 ± 0.03*,†	0.24 ± 0.13*,‡	0.32 ± 0.13†,‡
I_{LDLD}	0.44 ± 0.02*	0.37 ± 0.08*	0.39 ± 0.07
I_{RDLD}	0.30 ± 0.02	0.30 ± 0.03	0.30 ± 0.08
CI_{LD}	0.49 ± 0.02*	0.43 ± 0.07*,‡	0.52 ± 0.11‡

CI_{ED} = circularity index of main vortex during early diastole, CI_{LD} = circularity index of main vortex during late diastole, I_{DED} = index of the diameter of main vortex during early diastole, I_{DLD} = index of the diameter of main vortex, I_{LDED} = index of longitudinal distance of main vortex during early diastole, I_{LDLD} = index of longitudinal distance of main vortex, I_{LED} = index of the length of main vortex during early diastole, I_{LLD} = index of the length of main vortex, I_{RDED} = radial distance index of main vortex during early diastole, I_{RDLD} = radial distance index of main vortex, post-op = patient after operation, pre-op = patient before operation.

$P < .05$ is significant.

* Pro-op versus normal.

† Post-op versus normal.

‡ Post-op versus pre-op.

vortex will reduce cardiac work efficiency.[22] Therefore, the change of vortex can reflect the change of fluid in early left ventricular dysfunction. In addition, the asymmetry of vortex inside normal LV formed during diastole is essential to augment cardiac performance.[23,24] Once the normal asymmetry structure of the vortex in the LV is changed, it will lead to cardiac insufficiency.[24] In TA patients, due to the change of ventricular shape and irregular enlargement, with volume overload, the LV became more symmetric, resulting in the blood directly flow toward the apex and fanned out, causing vortices to be smaller and closer to the mitral annulus, failed to form a large whirlpool, not conducive to effective energy transformation. The change of the shape and location of the vortex showed scattered blood flow in the LV, which reflected the abnormality of the cardiac diastolic function of TA.

In this first report of using CFD on TA patients, CFD simulation simplified LV geometry without detailed delineation of papillary muscles and valves, but the good agreements between CFD reconstructed models and ECHO measured values, demonstrated the ability of CFD in accurately evaluating the anatomic abnormalities of TA. Furthermore, CFD demonstrated convenience in providing detailed information about intraventricular flow pattern. The change of existence and shape of vortex in pre-op and post-op TA patients suggested the capability of CFD to detect the surgical alteration of the hemodynamics in the LV, which can be further utilized in other congenital cardiac conditions. This initial CFD study in TA patients did not present a long-term follow-up result to reveal the benefit of different intraventricular flow patterns due to the varied follow-up period; however, CFD can definitely be applied to patients who underwent surgery for long-term follow-ups.

Acknowledgments

We express our great gratitude for the support of the National Nature Science Foundation of China [grant number 81501558], the Project-sponsored by the Scientific Research Foundation for the Returned Overseas Chinese Scholars, State Education Ministry [grant number 20144902], the Programs of the Shanghai Science and Technology Commission [grant number 14411968900], the Biomedical and Engineering (Science) Interdisciplinary Study Fund of Shanghai Jiaotong University [grant number YG2014MS63], the Project funded by China Postdoctoral Science Foundation [grant number 2014T70420], the Programs of the Shanghai Science and Technology Commission [grant number 14411961700], an Innovation Program of the Shanghai Municipal Education Commission [grant number 13ZZ081], the Fund of Shanghai Jiao-Tong University School of Medicine [grant number 14XJ10039], and the clinical science and technology innovation project of Shanghai Shen Kang Hospital Development Center [grant number SHDC22015019].

References

[1] Cohn JN, Ferrari R, Sharpe N. Cardiac remodeling—concepts and clinical implications: a consensus paper from an international forum on cardiac remodeling. J Am Coll Cardiol 2000;35:569–82.

[2] d'Udekem Y, Iyengar AJ, Cochrane AD, et al. The Fontan procedure: contemporary techniques have improved long-term outcomes. Circulation 2007;116:I157–64.

[3] Khairy P, Fernandes SM, Mayer JE, et al. Long-term survival, modes of death, and predictors of mortality in patients with Fontan surgery. Circulation 2008;117:85–92.

[4] Kheradvar A, Houle H, Pedrizzetti G, et al. Echocardiographic particle image velocimetry: a novel technique for quantification of left ventricular blood vorticity pattern. J Am Soc Echocardiogr 2010;23:86–94.

[5] Hayashi T, Itatani K, Inuzuka R, et al. Dissipative energy loss within the left ventricle detected by vector flow mapping in children: normal values and effects of age and heart rate. J Cardiol 2015;66:403–10.

[6] Markl M, Frydrychowicz A, Kozerke S, et al. 4D flow MRI. J Magn Reson Imaging 2012;36:1015–36.

[7] Lau KD, Figueroa CA. Simulation of short-term pressure regulation during the tilt test in a coupled 3D–0D closed-loop model of the circulation. Biomech Model Mechanobiol 2015;14:915–29.

[8] Kung E, Baretta A, Baker C, et al. Predictive modeling of the virtual Hemi-Fontan operation for second stage single ventricle palliation: two patient-specific cases. J Biomech 2013;46:423–9.

[9] Le TB, Sotiropoulos F. On the three-dimensional vortical structure of early diastolic flow in a patient-specific left ventricle. Eur J Mech B Fluids 2012;35:20–4.

[10] Mangual JO, Kraigher-Krainer E, De Luca A, et al. Comparative numerical study on left ventricular fluid dynamics after dilated cardiomyopathy. J Biomech 2013;46:1611–7.

[11] Seo JH, Mittal R. Effect of diastolic flow patterns on the function of the left ventricle. Phys Fluids 2013;25:110801.

[12] Lang RM, Badano LP, Mor-Avi V, et al. Recommendations for cardiac chamber quantification by echocardiography in adults: an update from the American Society of Echocardiography and the European Association of Cardiovascular Imaging. Euro Heart J Cardiovasc Imaging 2015;16:233–71.

[13] Nagueh SF, Appleton CP, Gillebert TC, et al. Recommendations for the evaluation of left ventricular diastolic function by echocardiography. Eur J Echocardiogr 2009;10:165–93.

[14] Domenichini F, Querzoli G, Cenedese A, et al. Combined experimental and numerical analysis of the flow structure into the left ventricle. J Biomech 2007;40:1988–94.

[15] Doenst T, Spiegel K, Reik M, et al. Fluid-dynamic modeling of the human left ventricle: methodology and application to surgical ventricular reconstruction. Ann Thorac Surg 2009;87:1187–95.

[16] Saber NR, Wood NB, Gosman A, et al. Progress towards patient-specific computational flow modeling of the left heart via combination of magnetic resonance imaging with computational fluid dynamics. Ann Biomed Eng 2003;31:42–52.

[17] Watanabe H, Sugiura S, Kafuku H, et al. Multiphysics simulation of left ventricular filling dynamics using fluid-structure interaction finite element method. Biophys J 2004;87:2074–85.

[18] Eicken A, Petzuch K, Marek J, et al. Characteristics of Doppler myocardial echocardiography in patients with tricuspid atresia after total cavopulmonary connection with preserved systolic ventricular function. Int J Cardiol 2007;116:212–8.

[19] Khairy P, Poirier N, Mercier L-A. Univentricular heart. Circulation 2007;115:800–12.

[20] Tomkiewicz-Pająk L, Hoffman P, Trojnarska O, et al. Cardiac surgery long-term follow-up in adult patients after Fontan operations. Kardiochir Torakochir Polska 2013;10:357–63.

[21] Gentles TL, Mayer JEJr, Gauvreau K, et al. Fontan operation in five hundred consecutive patients: factors influencing early and late outcome. J Thorac Cardiovasc Surg 1997;114:376–91.

[22] Konstam MA, Kramer DG, Patel AR, et al. Left ventricular remodeling in heart failure. JACC Cardiovasc Imaging 2011;4:98–108.

[23] Kilner PJ, Yang G-Z, Wilkes AJ, et al. Asymmetric redirection of flow through the heart. Nature 2000;404:759–61.

[24] Pedrizzetti G, Domenichini F. Nature optimizes the swirling flow in the human left ventricle. Phys Rev Lett 2005;95:108101.